10-2004

Wide Angle Decentered Lens Beam Steering for Infrared Countermeasures Applications

Jennifer L. Gibson
Anteon Corporation

Bradley D. Duncan
University of Dayton, bduncan1@udayton.edu

Edward A. Watson
Wright Laboratory

John S. Loomis
University of Dayton, jloomis1@udayton.edu

Wide-angle decentered lens beam steering for infrared countermeasures applications

Jennifer L. Gibson*
Anteon Corporation
5100 Springfield Pike
Suite 509
Dayton, Ohio 45431

Bradley D. Duncan, MEMBER SPIE
University of Dayton
Electro-Optics Program
300 College Park
Dayton, Ohio 45469-0245
E-mail: brad@udayton.edu

Edward A. Watson, FELLOW SPIE
Air Force Wright Laboratory
EO Technology Division
2241 Avionics Circle
Wright Patterson Air Force Base,
Ohio 45433-7304

John S. Loomis
University of Dayton
ECE Department
300 College Park
Dayton, Ohio 45469-0226

Abstract. A beam-steering system consisting of three cemented achromatic doublets is presented. Intended for use in IR countermeasure applications, our system is designed to operate over the 2- to 5-μm spectrum with minimum angular dispersion. We show that dispersion can be minimized by using doublet lenses fashioned from AMTIR-1 and germanium. Our system is designed to be compact and lightweight, with no internal foci, while allowing steering to ± 22.5 deg. We also maintain a minimum 2-in. clear aperture for all steering angles, and a nominal divergence of 1 mrad. Plane wave and Gaussian beam analyses of our system are presented.
[DOI: 10.1117/1.1789137]

Subject terms: infrared countermeasures; decentered lenses; beam steering; achromatic doublets; dispersion correction.

Paper 030563 received Nov. 10, 2003; revised manuscript received Feb. 27, 2004; accepted for publication Mar. 31, 2004.

1 Introduction

Optical beam steering has applications in many diverse technologies, including ladar, optical communications, optical interconnects, and spatial light modulator addressing.[1] Recently, several beam-steering methods have been investigated, as is summarized in the following. Of particular interest to this research have been methods involving decentered lens elements and arrays.[2–7] Specifically, the research presented herein focuses on an achromatic decentered lens approach for IR countermeasures (IRCM) applications.

Current optical sensor and IRCM systems are often severely limited in performance and cost by large mechanical beam-steering devices; e.g., dual-axis gimbaled mirror systems. Although this technology is now quite mature, there are clear limitations resulting from the physical size, weight, and power requirements of such beam-steering mechanisms, and the fact that most systems do not lend themselves to highly accurate, rapid random pointing.[2] Included among the many other methods of optical beam steering that have been investigated are the use of acousto-optic and/or electro-optic cells, and the use of rotating achromatic prisms.[8,9] More recent developments include the use of dynamic gratings and decentered microlens arrays, both of which involve an optical phased array approach to beam steering. This paper expands on the decentered lens approach. Specifically, a cascade of three aspheric achromatic lenses, two of which are decentered with respect to the other, is investigated in a proof-of-concept design. We see that this technique presents a highly promising solution to the beam-steering problem for airborne optical sensor and IRCM applications.

As expected, optical phased-array technology has the potential to overcome many of the problems presented by traditional beam-steering methods. Microlens arrays, for example, have the advantage of being lightweight.[1] Also, the amount of decenter required to obtain a large steering angle is typically fairly small due to their small focal lengths, often of the order of a millimeter or less.[3,5] However, the periodic structure of the arrays makes the output beam analogous to that of a blazed grating, resulting in the undesired diffraction of light into spurious directions and multiple beam orders.[3,5] This also creates blind spots into which the system is unable to steer energy. In addition, wide-angle beam steering with microlens arrays often requires lenses with small f-numbers, which are generally difficult to design. Furthermore, although some solutions have been proposed to decrease dispersion in a system of microlens arrays,[7] the current technology is generally quite dispersive.

To address these limitations, a system of macroscopic lenses is considered here. Although macroscopic lenses are not generally as small as an array of microlenses, we show that they do provide for a fairly compact beam-steering system overall. They also enable an achromatic design resulting in very low dispersion over a broad spectral band.

*Former address: University of Dayton, Electro-Optics Program, 300 College Park, Dayton, OH.

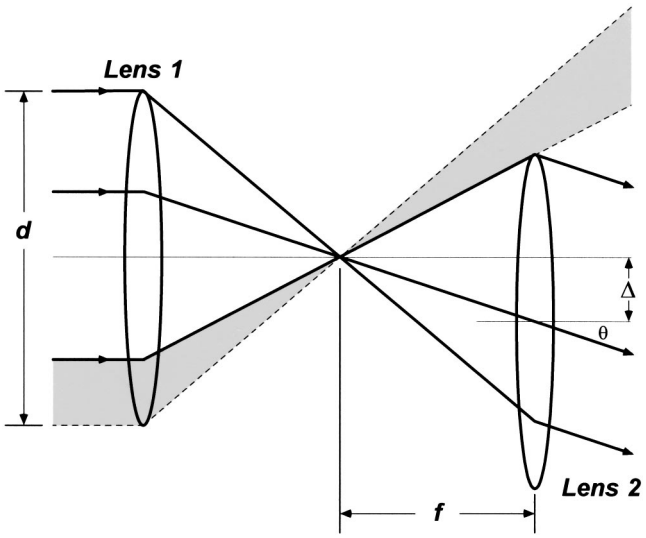

Fig. 1 Simple beam-steering system consisting of two identical thin lenses separated by two focal lengths. Displacing the second lens steers the beam of light, yet introduces loss due to vignetting.

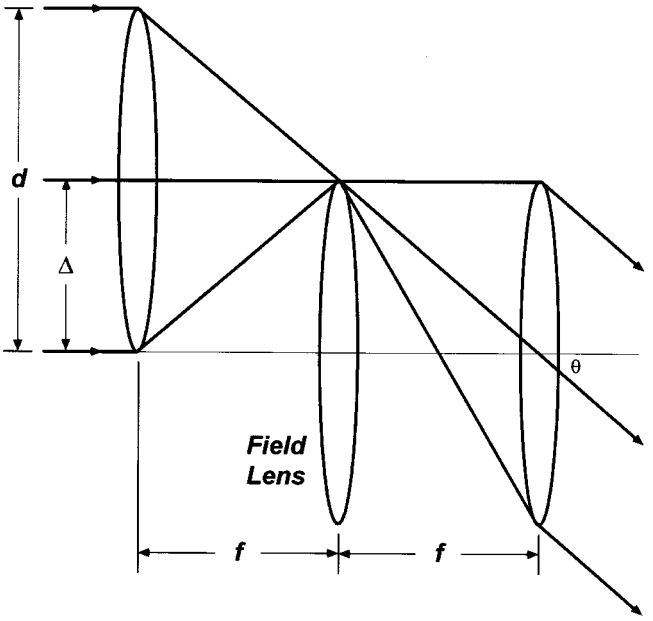

Fig. 2 Field lens can be used to eliminate vignetting, thereby maximizing throughput.

Furthermore, the use of macroscopic lenses enables us to avoid all blind spots while also enabling the use of lenses with manageable f-numbers.

We designed our beam-steering system with the following considerations in mind. Of greatest importance was to limit the steering angle dispersion, over the 2 to 5-μm midwave IR (MWIR) spectrum of interest, to less than 1 mrad. This was achieved through the development of appropriate achromatic doublet lenses, as discussed in Sec. 3. In addition, a 2-D wide-angle field of regard ($\sim$22.5 deg) was desired, while a clear aperture of approximately 2 in. was maintained to enable the system to act as both a transmitter and a large-area receiver. Furthermore, an outgoing beam divergence of 1 mrad was chosen to enable an appreciable broad optical footprint at an estimated target range of 6 to 10 km. To avoid any power-handling issues, we also designed the system to be free of internal foci. Last, we desire the final design to be as compact and lightweight as possible to facilitate a rapid random pointing capability. As a result, the thickness and diameter of each lens was carefully considered and minimized throughout the optimization process. Section 5 discusses some practical steps taken to both minimize the weight of our system and also simplify the fabrication of the lenses.

2 Geometric Analysis

The concept of beam steering using decentered lenses is conveniently understood by first considering two identical decentered simple lenses, as shown in Fig. 1, the first of which is illuminated by an infinite uniform plane wave. The incoming collimated wavefront is focused to a point in the back focal plane of the first lens, while the second lens is situated so that its front focal plane coincides with the back focal plane of the first lens. The decentered second lens then recollimates the exiting light, but the beam is directed to a nonzero steering angle. The angle θ into which the output wave is steered can be determined if the focal length f and the translation distance from the optical axis Δ are known. As can be seen, the following simple trigonometric relationship exists between f, Δ, and θ:

$$\theta = \tan^{-1}\left(\frac{\Delta}{f}\right). \tag{1}$$

Notice in Eq. (1) that as Δ increases, θ increases. However, for practical implementation, Δ is limited by the size of the lens, the maximum value being one half the lens diameter, or $d/2$. Therefore, the maximum steering angle is given by

$$\theta_{\max} = \tan^{-1}\left(\frac{d}{2f}\right) = \tan^{-1}\left(\frac{1}{2f/\#}\right), \tag{2}$$

where $f/\#$ is the lens f-number. Clearly, the $f/\#$ must be as small as possible to maximize the steering angle. For example, to achieve our maximum desired steering angle of 22.5 deg, an $f/\#$ of 1.2 would be required. This can introduce many design problems because lenses with small f-numbers typically exhibit large amounts of spherical and other aberrations.[10]

The use of paired lenses results in additional difficulties that must be overcome. As seen in Fig. 1, as the beam of light is steered off axis, some light is lost from the system due to vignetting, an effect that is most appreciable at large steering angles. To address this issue a field lens is inserted between the entrance and exit lenses at their common focal planes, as shown in Fig. 2. This creates a unity fill factor at the output of the cascaded lenses for all steering angles, thereby optimizing the throughput of the system.[11]

A complication involving the three-lens system of Fig. 2 is the presence of the internal focus at the field lens. An internal focus is undesirable due to the amount of power that would be concentrated at the focus. This concern was considered such a priority that an internal focus of any

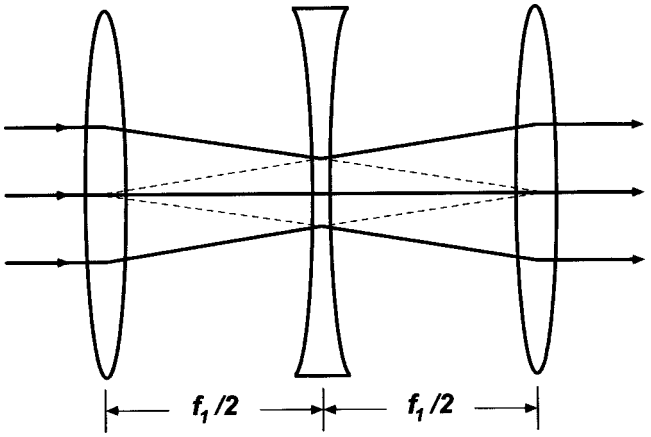

Fig. 3 Three-lens system consists of two identical positive lenses separated by a negative field lens. Assuming thin lenses, the focal length of the negative lens is one fourth that of the positive lenses.

kind, even in air, was determined to be unacceptable in our beam-steering system. As a result, a new system configuration was considered in which the positive field lens was replaced with a negative field lens.

The basic geometry of our modified three-lens beam-steering system is seen in Fig. 3. This design consists of two identical positive lenses placed one focal length apart. The negative field lens, placed halfway between the two positive lenses, must then have a focal length equal to one fourth that of the positive lenses. This can be verified using the thin lens equation; that is,

$$\frac{1}{f_2}=\frac{-2}{f_1}+\frac{-2}{f_1}=\frac{-4}{f_1}\Rightarrow f_2=\frac{-f_1}{4}, \tag{3}$$

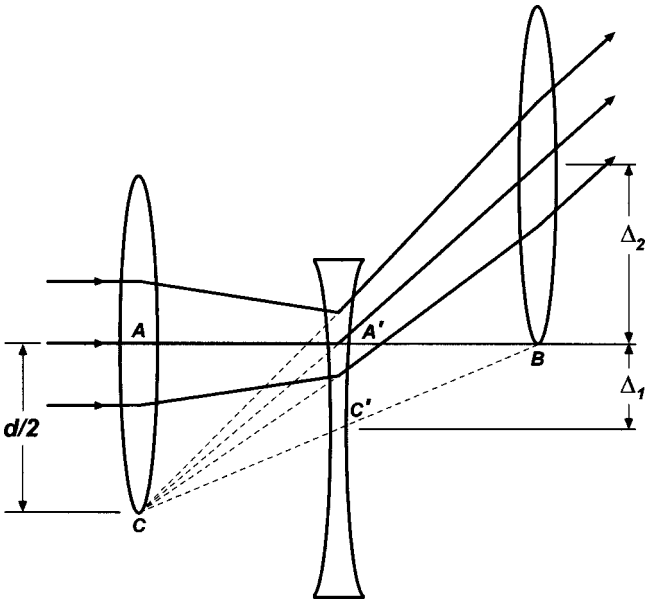

Fig. 4 System shown at the maximum allowable steering angle. A general steering angle relationship is dependent on the diameter of the lens d and the displacements of the field and exit lenses Δ_1 and Δ_2, respectively.

where f_1 is the focal length of the positive lenses and f_2 is the focal length of the negative lens.[10] This system can then be used to steer a beam of light by displacing the field and exit lenses in opposing directions, as seen in Fig. 4. However, the steering angle relationship for this system is slightly different from that expressed in Eq. (1). The general relationship is readily shown to be

$$\theta=\tan^{-1}\left(\frac{2\Delta_1+\Delta_2}{f_2}\right). \tag{4}$$

Now, we wish to utilize the central portion of the exit lens whenever possible in an attempt to minimize aberrations. The relationship between triangles ABC and $A'BC'$ in Fig. 4 can be used to determine the relative displacement of the field and exit lenses so that this occurs for all steering angles. Because these triangles are similar, the relationship

$$\frac{\Delta_1}{f_1/2}=\frac{d/2}{f_1}=\frac{\Delta_2}{f_1} \tag{5}$$

exists, indicating that $\Delta_2=2\Delta_1$. We also see that the maximum displacement of the exit lens is one half its diameter, i.e., $\Delta_2=d/2$, so that the maximum steering angle is

$$\theta_{\max}=\tan^{-1}\left(\frac{\Delta_2}{f_1/2}\right)=\tan^{-1}\left(\frac{d/2}{f_1/2}\right)$$
$$=\tan^{-1}\left(\frac{d}{f_1}\right)=\tan^{-1}\left(\frac{1}{f/\#}\right), \tag{6}$$

under the assumption that the beam passes through the center of the exit lens. Therefore, to achieve a maximum steering angle of 22.5 deg, the $f/\#$ of the entrance and exit lenses must be equal to 2.41. This means that the field lens must then in turn have an $f/\#$ of approximately 0.60, a fact which may lead to excessive aberrations. However, to meet our exit beam divergence requirements we will see that we must often transmit a beam whose diameter is much smaller than the full clear aperture of 2 in. This will thus increase the effective $f/\#$s of the lenses in our system, at least for transmission, thereby greatly aiding in the design process.

Recall that our divergence requirement dictates that the full spread angle of the exiting beam remain within 1 mrad. Recall also that the diffraction-limited divergence angle for uniform plane wave transmission is defined as

$$\theta_{\mathrm{DL}}=\frac{2.44\lambda}{D}, \tag{7}$$

where λ is the wavelength, and D is diameter of the aperture.[12] For a 2-in. clear aperture and a wavelength of 3.5 μm, the diffraction-limited divergence is 0.17 mrad. Our divergence specification is then nearly six times the diffraction limit, yielding a spot diameter of approximately 6 m at an operating distance of 6 km. This specification becomes very important in judging the performance of our system, as we see that both the beam size and the presence of aberrations strongly affect the divergence of the system.

Table 1 Materials considered and their Abbe numbers.

Material	Abbe Number
Al_2O_3	6.135
AMTIR-1	76.923
BaF_2	33.333
CaF_2	16.667
CdTe	47.619
Ge	30.303
IRGN6	7.634
LiF	6.897
MgO	9.524
ZnS	66.667
ZnSe	83.333

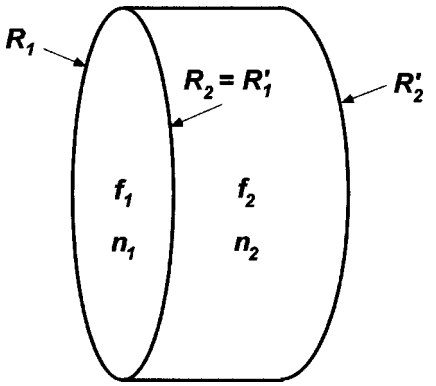

Fig. 5 General Fraunhoffer doublet lens with various parameters defined.

However, it is also important to ensure that the divergence is not made too small. If the output beam footprint is not large enough, we run the risk of missing our target. Therefore, we attempt to design our system so that most of the output light falls just within a full divergence angle of 1 mrad.

3 Design Procedure

The initial step in developing our system was to choose materials from which we would design our lenses. We accomplished this task by first designing a single achromatic doublet to minimize dispersion over the 2- to 5-μm range. Our goal was to design a cemented Fraunhoffer doublet lens in which a positive first component is followed by a negative second component. This is due to the fact that aberrations of a negative lens can often offset those of a positive lens.[10,13] The materials we considered, along with their Abbe numbers, are given in Table 1. Note that water soluble IR transmissive materials were not considered due to the atmospheric conditions under which our system is expected to operate. Furthermore, birefringent materials were not considered, as they would cause undesirable beam broadening in one direction.

Recall that the Abbe number, a common measure of dispersive power, is specified according to the relationship

$$V=\frac{n_c-1}{n_{\text{short}}-n_{\text{long}}}, \tag{8}$$

where n_{short} and n_{long} are the indices of refraction at the shortest and longest wavelengths of interest, while n_c is the index of refraction at the center of the spectral band over which our system will be expected to operate.[12] In our case, n_{short}, n_{long}, and n_c were evaluated at the MWIR wavelengths of 2, 5, and 3.5 μm, respectively. Now, it can be shown that the radii of curvature of a thin Fraunhoffer doublet, whose geometry is given in Fig. 5, satisfy the following relationships:

$$\frac{1}{R_1}-\frac{1}{R_2}=\frac{V_2}{f(V_2-V_1)(n_{1c}-1)} \quad \text{and}$$

$$\frac{1}{R_2'}-\frac{1}{R_2}=\frac{V_1}{f(V_1-V_2)(n_{2c}-1)}, \tag{9}$$

where f is the focal length of the overall doublet: R_1 is positive: R_2 and R_2' are negative; V_1 and V_2 are the Abbe numbers of the first and second components, respectively; and n_{1c} and n_{2c} are the indices of refraction at 3.5 μm for the first and second components. Similarly, by multiplying Eqs. (9) by (n_c-1), we find that the focal lengths of each component of the doublet satisfy the following relationships:[12]

$$\frac{1}{f_1}=\frac{V_2}{f(V_2-V_1)} \quad \text{and} \quad \frac{1}{f_2}=\frac{V_1}{f(V_1-V_2)}. \tag{10}$$

The optimum material combinations for the first and second components of the lens were determined by first identifying those material combinations that resulted in a doublet lens whose first element would be positive, followed by a negative second element. The most effective combination of materials was then defined as that yielding the smallest spot size at its focal point. To begin, we initially chose a lens diameter of 2 in. and an effective focal length of 100 mm, yielding a maximum potential steering angle of 26.9 deg according to Eq. (6). We then used the Abbe numbers given in Table 1 along with Eq. (10) to find combinations where $f_1>0$ and $f_2<0$. Assuming an initial value for R_1 of the order of 100 mm, Eqs. (9) were then used to find initial values for R_2 and R_2', with the constraint that $R_2<0$. We then used the automatic design option of the CODE V® software package to optimize the lens for minimum dispersion (CODE V® Version 9.1, Optical Research Associates, Pasadena, California). The minimum root mean square (rms) focal spot size for each allowable combination, found using the spot diagram option of CODE V®, is provided in Table 2. We found that the smallest spot size resulted from a combination of AMTIR-1 and germanium. While germanium is a common element, AMTIR-1 is a material produced by Amorphous Materials, Inc., having the chemical composition $Ge_{33}As_{12}Se_{55}$ (Amorphous Materials, Inc., Garland, Texas). Its name is an

Table 2 Resulting spot sizes for acceptable material combinations.

First Component	Second Component										
	Al_2O_3	LiF	IRGN6	MgO	CaF_2	Ge	BaF_2	CdTe	ZnS	AMTIR-1	ZnSe
ZnSe	0.53228	0.53888	0.53236	0.57654	0.53740	0.15752	0.53748	0.5271	0.52688	0.12991	
AMTIR-1	0.55499	0.56219	0.55549	0.55066	0.56166	**0.11316**	0.56178	0.12028	0.46742		
ZnS	0.58385	0.59310	0.67460	0.66901	0.59209	0.13348	0.59357	0.2772			
CdTe	0.59701	0.60825	0.60603	0.60190	0.61581	0.16979	0.61730				
BaF_2	1.90480	2.08110	1.66220	0.69804	2.07590	0.67036					
Ge	0.65760	0.67754	0.67330	0.67304	0.69162						
CaF_2	0.53183	2.48220	0.51573	0.37484							
MgO	0.9648	1.6933	1.6812								
IRGN6	0.96325	2.213									
LiF	2.41830										
Al_2O_3											
	rms Spot Size (mm)										

acronym standing for amorphous material transmitting IR radiation. For reference, the dispersion curves for these materials are provided in Fig. 6.

The dimensions of our optimized achromat are shown in Table 3. The headings in Table 3 correspond to those in CODE V®, where the *y* radius is the radius of curvature, and the *y* semiaperture is the height from the optic axis. As desired, the final optimized lens consists of a positive element followed by a negative element. This design was then used in CODE V® as the initial entrance and exit elements of our beam steering system. CODE V® was also used to design and optimize the field lens as a part of the overall system. Note that we initially assume identical entrance and exit lenses to achieve a unity fill factor in the simplest and most compact design possible.

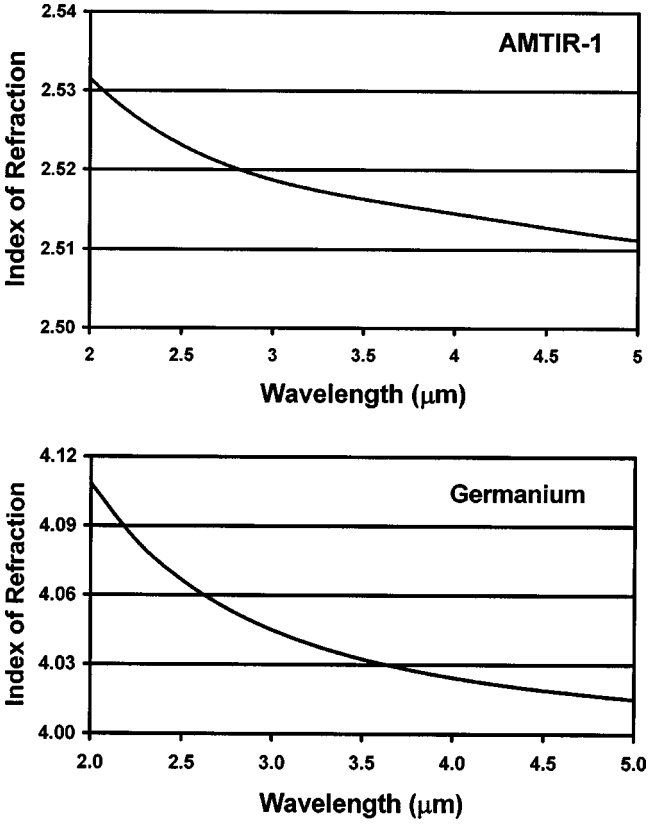

Fig. 6 Dispersion curves for the two materials used in our system: AMTIR-1 and Germanium.

Because our system is to be used as both a transmitter and receiver, it is important to understand certain characteristics of the transmitted and received beams. The system was generally designed to transmit up to a 1-in.-diam beam and to receive up to a 2-in. beam. While the transmitted beam will most likely have a Gaussian cross section, any received information will likely have a planar wavefront due to interaction with the target and the great distance it will have traveled before reaching our steering system. When receiving a 2-in. beam, the outermost portions of the lenses, which tend to introduce the most aberrations, will clearly be in use. Note, however, that our design is that of a nonimaging device. When used as a receiver, our system simply serves to steer the field of view from which a minimum 2-in. beam cross section can be intercepted. As such, when used as a receiver, only the ability to collect power and direct it to a photodetector is of importance, while aberrations are only of secondary concern. During transmission, however, we will utilize the more central portions of the lenses. In this case, aberrations are of greater concern, but only (as already discussed) to the extent that they affect the beam divergence angle. Nevertheless, to ensure that the system was optimized as both a transmitter and receiver,

Table 3 Optimized achromatic doublet dimensions.

Surface	*y* Radius (mm)	Thickness (mm)	Glass	*y* Semiaperture (mm)
Object	Infinity	Infinity		
Stop	84.43654	25.0000	AMTIR-1	25.4000
2	−485.9788	5.0000	Ge	25.4000
3	452.1207	80.2546		25.4000
4	Infinity	0.0000		25.4000

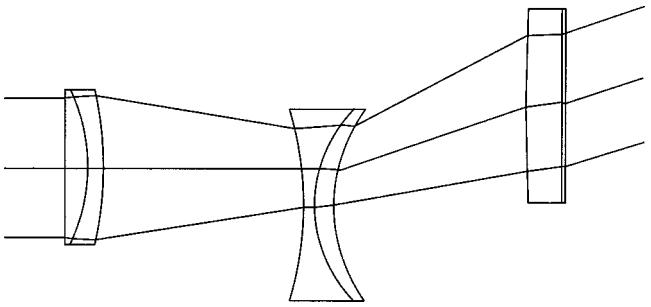

Fig. 7 Scaled diagram of optimized system at the maximum steering angle of 22.5 deg.

we designed the system in CODE V® as if it were transmitting a broadband 2-in. planar beam—the worst case scenario with respect to aberrations and dispersion. Consequently, this design step served to improve the more practical situation of transmitting a small Gaussian beam while also optimizing the reception of a 2-in. planar beam. In all cases, CODE V® was used to optimize the system by controlling the divergence while maximizing its steering angle. The results for transmitting both a 1-in. plane wave and a reduced-size Gaussian beam are presented in the following section. Some additional practical concerns are presented in Sec. 5.

4 Results

Our beam-steering system was optimized at many steering angles using the zoom lens option in CODE V®. This enabled us to specify several different positions for the field and exit lenses while maintaining a collimated output during optimization. The system was then continually modified using suggestions from the automatic design option to minimize aberrations and control the divergence of the output. After extensive automatic global and local CODE V® optimizations we settled on the system, shown to scale, in Fig. 7. The exact dimensions of this system are provided in Table 4. From Table 4 we see that the field lens and exit lenses were increased to a diameter of 70 mm to ensure that a 2-in. beam could be received at all steering angles without vignetting. However, it was only necessary to slightly increase the diameter of the entrance lens, as it always remains on-axis. We found that we were able to steer to the specified angle of 22.5 deg while staying within our divergence specifications. In addition, the length of the system was found to be 178.37 mm, while its height, at maximum displacement, is 135.36 mm.

Table 4 Dimensions of the optimized system.

Surface	*y* Radius (mm)	Thickness (mm)	Glass	*y* Semiaperture (mm)
Object	Infinity	Infinity		
Stop	Infinity	0.0000		12.70
2	−18362.3156	7.6762	AMTIR-1	26.00
3	−71.0844	6.3890	Ge	26.00
4	−112.2832	72.5428		26.00
5	−137.1835	3.0000	AMTIR-1	35.00
6	54.4808	7.8125	Ge	35.00
7	77.2541	66.2858		35.00
8	537.7414	13.0000	Ge	35.00
9	9953.718	1.6656	AMTIR-1	35.00
10	−6206.8429	30.0000		35.00
Image	Infinity	0.0000		120.00

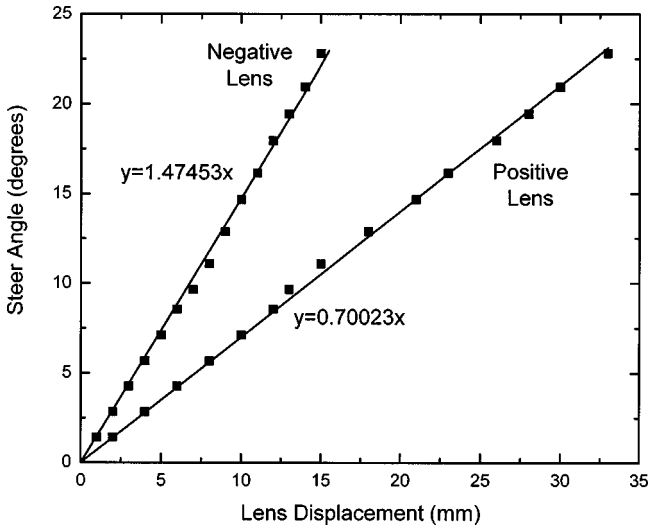

Fig. 8 Nearly 2:1 relationship exists between the magnitude of the displacements of the exit and field lenses for an optimized system output.

The displacement of the field and exit lenses, as a function of steering angle, is shown in Fig. 8. The linear trend lines in this figure demonstrate that the relationship between the displacements of the exit and field lenses is nearly 2 to 1, as evidenced by the slopes of 1.47 and 0.70. This supports the geometric theory presented earlier, where propagation through the central portions of the exit lens was assumed.

Spot diagrams for this system at 2 and 5 μm at a range of 6 km are provided in Fig. 9 under the assumption of a 1-in. plane wave transmission. The on-axis spot diagrams in Fig. 9(a) show evidence of slight chromatic aberrations, while the off-axis plots in Fig. 9(b), shown at a steering angle of 22.5 deg, demonstrate the existence of some residual coma. Next, encircled energy plots, also under the assumption of 1-in. plane wave transmission, are shown in Fig. 10 for the 2 and 5 μm wavelengths. The on-axis energy remaining within a 1 mrad divergence angle at a range of 6 km is about 98% at 2 μm, and 90% at 5 μm. At a steering angle of 22.5 deg, this percentage remains at 98% for a wavelength of 2 μm, and decreases to an acceptable 63% at 5 μm.

The next step was to evaluate our system under the assumption of Gaussian beam transmission. It can be shown that well beyond the Rayleigh range the full angular spread of a Gaussian beam in air is[14]

$$2\theta_{1/e}=\frac{2\lambda}{\pi w_o}. \tag{11}$$

Using this equation, a waist of 2 mm would be required to maintain a divergence of 1 mrad at 3.5 μm. Therefore, a

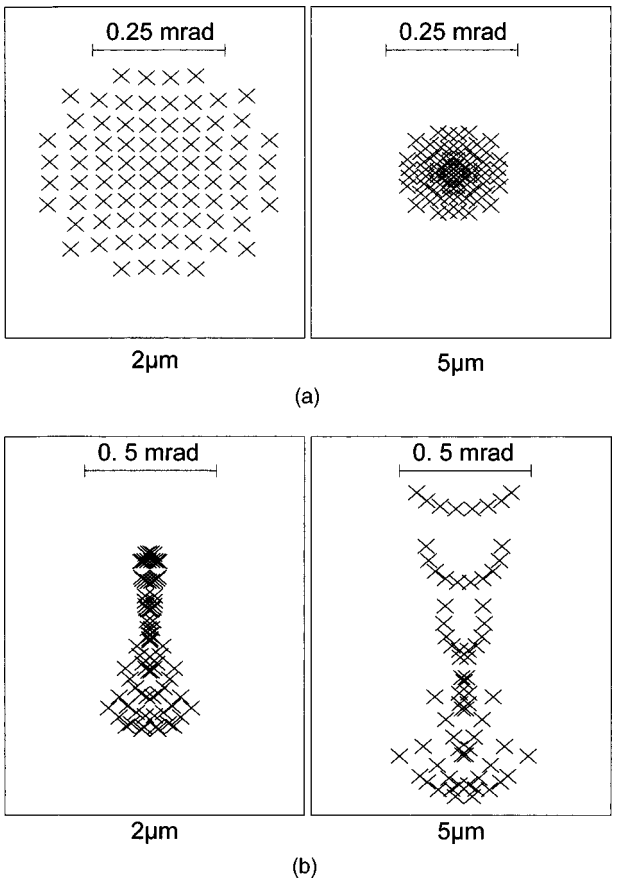

Fig. 9 Spot diagrams at a range of 6 km (a) on-axis and (b) at 22.5 deg. Chromatic aberrations are seen both on- and off-axis; coma is seen at 22.5 deg.

Gaussian beam with a waist of 2 mm was initially propagated through our three-lens system. The value of the beam waist was then varied until a far-field divergence of 1 mrad was achieved. We found that this occurred for a beam waist of 4.1 mm.

The resulting on-axis Gaussian beam profiles for 2 and 5 μm are provided in Fig. 11(a) at a distance of 6 km. We see that very little distortion occurs on-axis. Similarly, the beam profiles at the maximum steering angle of 22.5 deg are seen in Fig. 11(b). Here we see that there is some spreading of the beam in one direction, again suggesting the presence of some residual coma.

The encircled energy plots for Gaussian wave transmission at a range of 6 km are shown in Fig. 12. We see that over 90% of the original energy remains within a divergence angle of 1 mrad on-axis. This is exceptional performance and will be quite sufficient for our purposes. Similarly, the encircled energy plots at the maximum steering angle of 22.5 deg indicate that at least 63% of the original energy remains within 1 mrad of divergence.

To investigate the success at eliminating chromatic aberrations, the angular dispersion at a nominal steering angle of 22.5 deg was determined by using CODE V® to find the exact steering angle at 2, 2.75, 3.5, 4.25, and 5 μm. The results are shown in Fig. 13. We see that the first-order angular dispersion (i.e., the slope of the steering angle

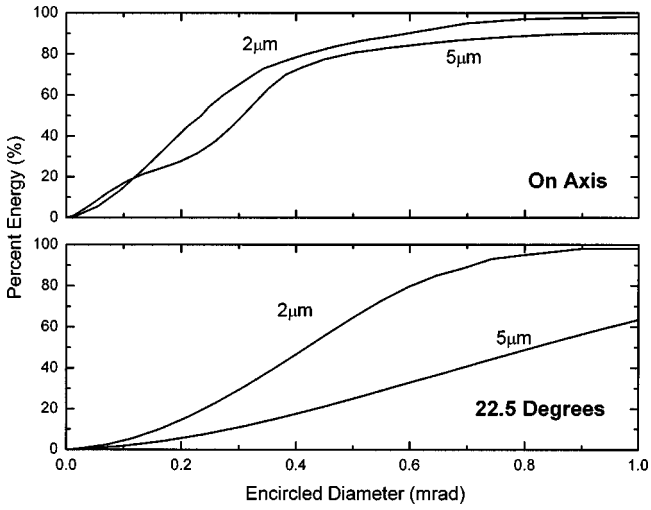

Fig. 10 For a planar input, the encircled energy within 1 mrad at a range of 6 km decreases from 90% on-axis to 63% at 22.5 deg for a source wavelength of 5 μm. At 2 μm, the encircled energy within 1 mrad remains above 95% for both cases.

curve) has been reduced to zero at 2.75, 3.5, and 4.4 μm. However, the maximum secondary angular dispersion occurs between 2.6 and 5 μm and is approximately 0.0372 deg, or 0.649 mrad. This is well within our 1-mrad specification.

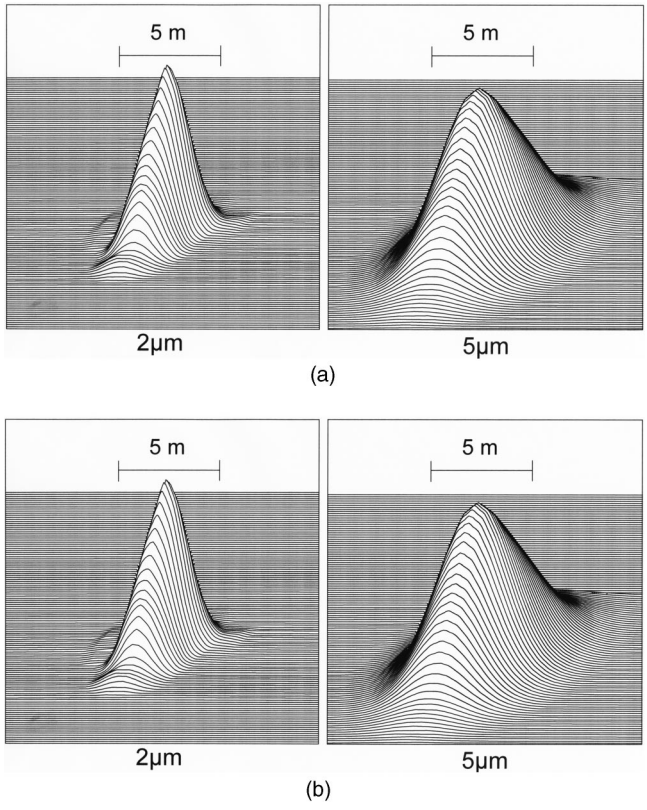

Fig. 11 Gaussian beam profiles at a range of 6 km for 2 and 5 μm (a) on-axis and (b) at 22.5 deg.

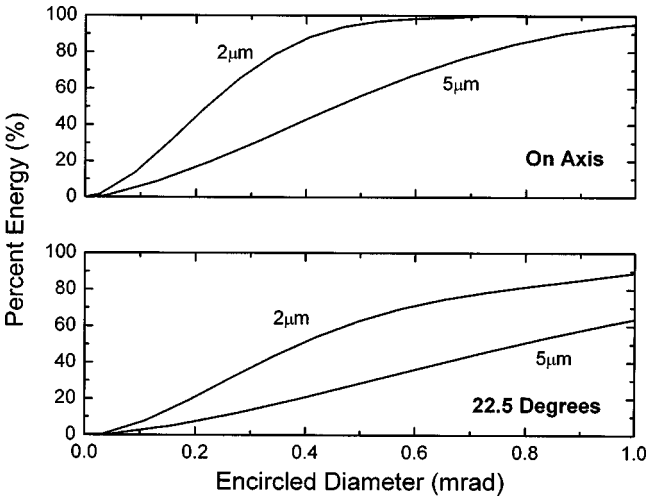

Fig. 12 For a Gaussian input, the encircled energy within 1 mrad at a range of 6 km decreases from 95% on-axis to 63% at 22.5 deg for a source wavelength of 5 μm. At 2 μm, the encircled energy within 1 mrad remains above 90% for both cases.

5 Practical Concerns

There are practical concerns involving the entrance lens of our system. For example, as shown in Table 4 the magnitude of the radius of curvature of the first surface is extremely large. As such, this surface contributes little optical power to the overall system. In addition, from a fabrication standpoint, it would be advantageous to make the radius of curvature at this surface infinite. Other fabrication concerns pertain to the exit lens in the system. As can be seen in Table 4, this lens also contains two surfaces of extremely high radii of curvature. Once again, it would be advantageous to set these radii of curvature to infinity.

Another concern involves the thickness of the second component of the exit lens. This component might be difficult to fabricate because it is so thin, and it is thus desirable to eliminate it altogether. Recall that the second component of the exit lens is made of AMTIR-1, which has an index of refraction of approximately 2.5. Because this component is so thin and the index of refraction is relatively small with respect to the Ge element, it is reasonable to assume that disposing of this element may not affect the overall system performance dramatically. Finally, the accuracy of each dimension was reduced to one decimal point, instead of the four decimal points seen in Table 4. This would be a more realistic expectation when manufacturing these lenses.

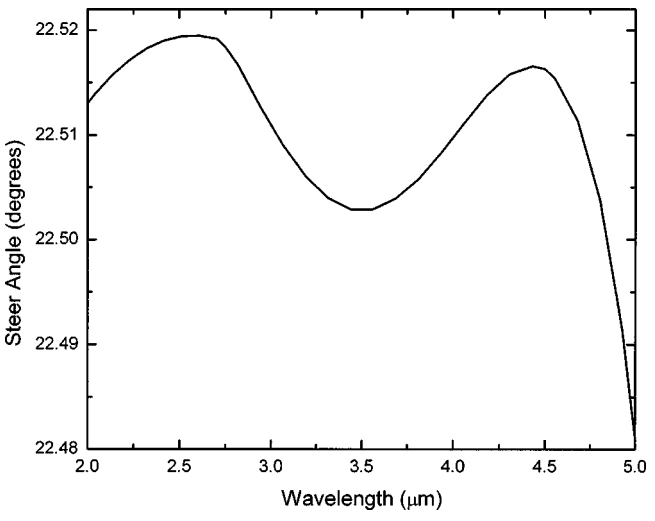

Fig. 13 Maximum angular dispersion, occurring between the 2.6 and 5 μm wavelengths, is about 0.0372 deg, or 0.649 mrad.

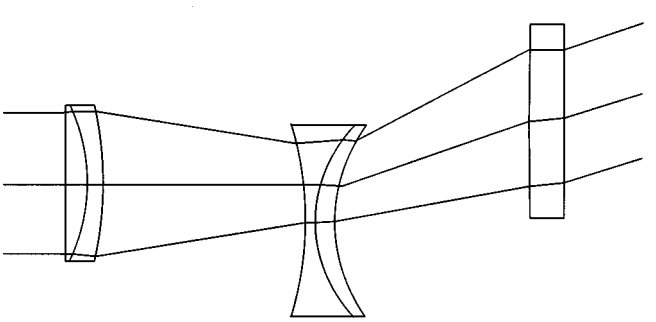

Fig. 14 Scaled diagram of the modified system at the maximum steering angle of 22.5 deg.

To summarize, the following practical changes where made to the original system dimensions:

1. The first radius of curvature of the entrance lens was changed to infinity.
2. The second radius of curvature of the exit lens was changed to infinity.
3. The final component of the exit lens was eliminated.
4. The accuracy of each dimension was reduced to one decimal place.

The modified system is shown to scale in Fig. 14, while the dimensions for this system are listed in Table 5. The encircled energy plots on-axis and at the maximum steering angle for Gaussian beam inputs are seen in Fig. 15. On-axis, we see that the encircled energy within one mrad remains above 90% at a range of 6 km. Off-axis, these numbers decrease to 63% at 5 μm and 95% at 2 μm. It is thus evident that the divergence of our system is only minimally compromised by our modifications.

Table 5 Modified system dimensions.

Surface	*y* Radius (mm)	Thickness (mm)	Glass	*y* Semiaperture (mm)
Object	Infinity	Infinity		
Stop	Infinity	0.0		12.7000
2	Infinity	7.7	AMTIR-1	26.0000
3	−71.1	6.4	Ge	26.0000
4	−112.3	72.5		26.0000
5	−137.2	3.0	AMTIR-1	35.0000
6	54.5	7.8	Ge	35.0000
7	77.3	66.3		35.0000
8	537.7	13.0	Ge	35.0000
Image	Infinity	0.0		120.0000

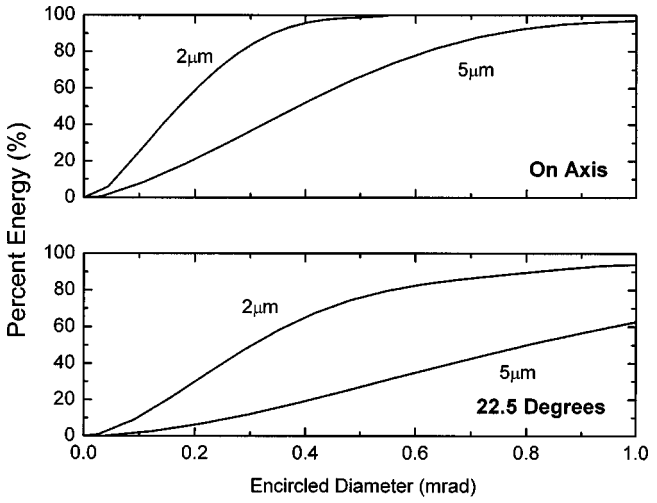

Fig. 15 Similar to Fig. 12, for a Gaussian input, the encircled energy within 1 mrad for the modified system at a range of 6 km decreases from 98% on-axis to 63% at 22.5 deg at a source wavelength of 5 μm. Again, the encircled energy at 2 μm within 1 mrad remains above 95% for both cases.

The angular dispersion for this system is seen in Fig. 16. Here, we see an overall decrease in the maximum steering angle by approximately 0.06 deg, as compared to Fig. 13. This is inconsequential. First-order angular dispersion has been reduced at 2.5, 3.3, and 4.25 μm. The maximum secondary angular dispersion occurs between 2.5 and 5 μm and has increased only slightly to 0.0377 deg, or 0.658 mrad. This continues to remain well within our 1-mrad angular dispersion specification.

We thus see that the minor alterations already discussed can be made to the system without significantly affecting its performance. This is extremely useful because it will not only simplify the manufacturing processes to fabricate these lenses, but will also likely reduce manufacturing costs.

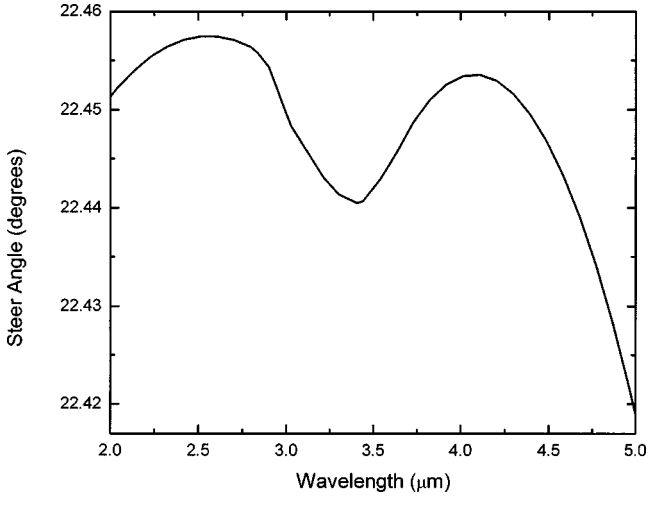

Fig. 16 Maximum angular dispersion for the modified system, occurring between the 2.5 and 5 μm wavelengths, is about 0.0377 deg, or 0.658 mrad.

6 Conclusions

We showed that a system of three cemented achromatic doublets enables us to eliminate many of the problems demonstrated by microlens arrays, such as the diffraction of light into spurious directions and multiple beam orders, blind spots, and large dispersion. While a field lens was used to allow for 100% throughput, power-handling issues were avoided by using a negative field lens to eliminate internal foci. After extensive CODE V® development, the resulting system design followed our geometric theory very closely, demonstrating a nearly 2 to 1 lens displacement ratio between the exit and field lenses. In addition, the dimensions of each lens were carefully considered, and slight modifications were made to aid in the fabrication process without compromising the performance of the system.

The design, consisting of the materials AMTIR-1 and germanium has an overall length of 178.37 mm and a height at maximum lens displacement of 135.36 mm. Furthermore, the use of achromatic doublets enabled a design with a maximum secondary angular dispersion of 0.658 mrad over the full 2 to 5-μm range. Spot diagrams showed the existence of residual coma at high steering angles, but these aberrations did not significantly compromise our beam divergence, and are therefore of less concern for this application. For a 1-in. plane wave input, at least 63% of the outgoing energy remained within a divergence of 1 mrad at the operating range of 6 km. In addition, for a Gaussian beam input it was shown that the system performance would be optimized with a beam waist of 4.1 mm. In this case, the amount of energy within a divergence angle of 1 mrad, at a range of 6 km, remains at least 63%. As we have shown, this design meets the requirements for our application.

Acknowledgments

This research has been supported in part by the U.S. Air Force and Opti-Metrics, Inc., through Contract No. F33615-00-D-J001. The authors would like to acknowledge the technical support department of Optical Research Associates, especially Dr. Bruce Jacobsen, for their assistance with CODE V® throughout this project.

References

1. E. A. Watson and L. J. Barnes, "Optical design considerations for agile beam steering," in *Laser Beam Propagation and Control*, H. Weichel and L. F. DeSandre, Eds., *Proc. SPIE* **2120**, 186–193 (1994).
2. P. F. McManamon, T. A. Dorschner, D. L. Corkum, L. J. Friedman, D. S. Hobbs, M. Holz, S. Liberman, H. Q. Nguyen, D. P. Resler, R. C. Sharp, and E. A. Watson, "Optical phased array technology," *Proc. IEEE* **84**(2), 268–298 (1996).
3. E. A. Watson, "Analysis of beam steering with decentered microlens arrays," *Opt. Eng.* **32**(11), 2665–2670 (1993).
4. E. A. Watson, L. J. Barnes, and A. J. Carney, "Application of dynamic gratings to broad spectral band beam steering," in *Laser Beam Propagation and Control*, H. Weichel and L. F. DeSandre, Eds., *Proc. SPIE* **2120**, 178–185 (1994).
5. W. Goltsos and M. Holz, "Agile beam steering using binary optics microlens array," *Opt. Eng.* **29**(11), 1392–1397 (1990).
6. E. A. Watson, W. E. Whitaker, C. D. Brewer, and S. R. Harris, "Implementing optical phased array beam steering with cascaded microlens arrays," *IEEE Aerospace Conf. Proc.* **3**, pp. 1433–1436 (2002).
7. K. M. Flood, B. Cassarly, C. Sigg, and J. M. Finlan, "Continuous wide angle beam steering using translation of binary microlens arrays and a liquid crystal phased array," in *Computer and Optically Formed Holographic Optics*, I. Cindrich and S. H. Lee, Eds., *Proc. SPIE* **1211**, 296–304 (1990).

8. J. D. Zook, ''Light beam deflector performance: a comparative analysis,'' *Appl. Opt.* **13**(4), 875–887 (1974).
9. B. D. Duncan, P. J. Bos, and V. Sergan, ''Wide angle achromatic prism beam steering for infrared countermeasures applications,'' *Opt. Eng.* **42**(4), 1038–1047 (2003).
10. W. J. Smith, *Modern Optical Engineering*, 3rd ed., pp. 61–90, McGraw Hill, New York (2000).
11. K. D. Möller, *Optics*, pp. 410–412, University Science Books, Mill Valley, CA (1988).
12. E. Hecht, *Optics*, pp. 228, 273, Addison Wesley Longman, New York (1998).
13. A. Nussbaum and R. A. Phillips, *Contemporary Optics for Scientists and Engineers*, Prentice-Hall, Englewood Cliffs, NJ (1976).
14. A. E. Seigman, *Lasers*, p. 352, University Science Books, Mill Valley, CA (1986).

Jennifer L. Gibson completed a 5-year program at the University of Dayton where she received her BS degree in electrical engineering in 2001 and her MS degree in electro-optics in 2003. She is currently an electro-optics engineer with Anteon Corp., where she is involved in research concerning photorefractive materials at the Air Force Research Laboratory.

Bradley D. Duncan received his PhD degree in electrical engineering from Virginia Polytechnic Institute and State University (Virginia Tech) in 1991, after which he joined the University of Dayton (UD) faculty. He is now a tenured (full) professor of electrical and computer engineering, with a joint appointment in the graduate Electro-Optics Program. Dr. Duncan's research interests and activities span a wide range of areas within the optical sciences, including the study of ladar systems, photorefractive applications, fiber optic sensor and system technology, integrated optics, nondestructive evaluation, and scanning and nonlinear optical image processing. He is a member of the OSA, SPIE, and ASEE and a senior member of IEEE. He has previously served as the book reviews editor for *Optical Engineering* and is the faculty advisor for both the University of Dayton student chapter of the OSA and EΔT, UD's engineering social fraternity. Dr. Duncan directs the research conducted in the UD's National Science Foundation (NSF) Photonics Laboratory, and in 1998 he won the Engineering Best Professor of the Year award.

Edward A. Watson is the technical advisor of the Electro-Optical Technology Division of the Air Force Research Laboratory. He joined the laboratory in 1991 and has been involved in research in active and passive electro-optic sensors, including the application of dynamic diffractive optical components to the agile steering and shaping of monochromatic and polychromatic light beams, the development of multiphenomenology laser radar imagers, and modeling of aliasing and blurring in sampled imagery. He is also an adjunct assistant professor of electrical engineering at the Air Force Institute of Technology. He has a PhD degree in optics from the University of Rochester, and an MS degree in optical sciences and a BS degree in physics from the University of Arizona. He is a Fellow of the SPIE.

John S. Loomis has been a research optical physicist and professor of electro-optics at the University of Dayton since 1979. His research interests include image analysis, computer graphics, geometric optics, interferometry, and ellipsometry. He has authored computer programs in interferogram reduction, optical design, and thin-film design and analysis. Dr. Loomis received his BS degree in physics from Case Institute of Technology, his MS degree in physics from the University of Illinois, and his PhD degree in optical sciences from the University of Arizona. He is a member of the Machine Vision Association of the Society of Manufacturing Engineers, the Association for Computing Machinery, OSA, and SPIE.